

Copyright © 1996, by the author(s).  
All rights reserved.

Permission to make digital or hard copies of all or part of this work for personal or classroom use is granted without fee provided that copies are not made or distributed for profit or commercial advantage and that copies bear this notice and the full citation on the first page. To copy otherwise, to republish, to post on servers or to redistribute to lists, requires prior specific permission.

**RF PLASMA POTENTIAL AND SURFACE  
TEMPERATURE MEASUREMENTS IN AN  
INDUCTIVELY COUPLED PLASMA SOURCE**

by

Gianluca Gregori and Michael A. Lieberman

Memorandum No. UCB/ERL M96/14

10 April 1996

COVER PAGE

**RF PLASMA POTENTIAL AND SURFACE  
TEMPERATURE MEASUREMENTS IN AN  
INDUCTIVELY COUPLED PLASMA SOURCE**

by

Gianluca Gregori and Michael A. Lieberman

Memorandum No. UCB/ERL M96/14

10 April 1996

**ELECTRONICS RESEARCH LABORATORY**

College of Engineering  
University of California, Berkeley  
94720

# RF Plasma Potential and Surface Temperature Measurements in an Inductively Coupled Plasma Source

Gianluca Gregori<sup>1</sup> and Michael A. Lieberman<sup>2</sup>

<sup>1</sup>Department of Nuclear Engineering,  
University of Bologna,  
Bologna, Italy

<sup>2</sup>Department of Electrical Engineering and Computer Sciences,  
University of California at Berkeley,  
Berkeley, CA 94720

## Abstract

The RF potential and temperature of a probe inserted into an argon plasma generated in a Transformer Coupled Plasma (TCP) source was measured. The plasma was driven by a 13.56 MHz RF power supply connected to a three turn coil that was inductively coupled to the plasma across a 2.5 cm thick quartz dielectric window. The coil was not electrostatically shielded from the plasma. The input power was varied from 50 to 500 watts and the argon gas pressure was varied from 10 to 50 mTorr. The results show that the RF plasma potential is fairly independent of pressure and increases weakly with input power, varying from 5-8 volts under capacitively coupled conditions (50-200 watts) to 8-15 volts under inductively coupled conditions (300-500 watts). Similarly, the temperature measurement reveals that the temperature increases with power and pressure to as high as 355 degrees Celsius.

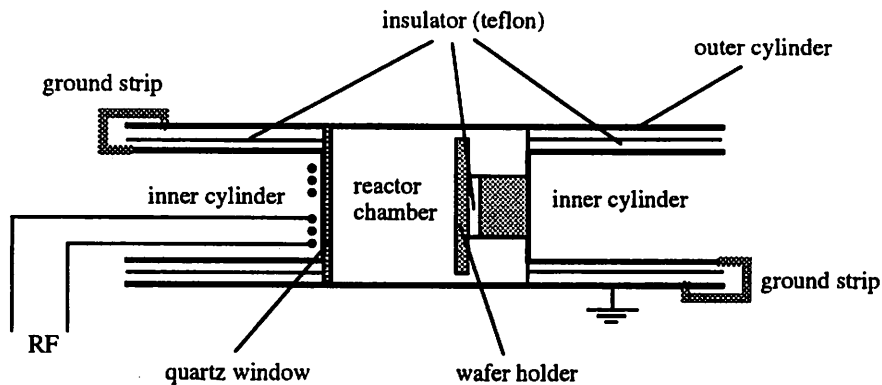


Figure 1: TCP schematic

## 1 Introduction

Plasma discharges are a fundamental tool in semiconductor manufacturing and other materials processing. Inductive discharges are commonly used in this technology since they have a simple design and are driven by RF rather than microwaves, and have no applied dc magnetic fields. These kind of discharges are referred to as TCPs (transformer coupled plasmas) or ICPs (inductive coupled plasmas). A detailed description of TCPs can be found in patents filed by Coultras and Keller [1] and by Ogle [2]; in particular, a specific characterization of the machine used is given by Wainman *et al.* [3]. Figure 1 shows a schematic of this machine.

The measurement of the plasma potential is one characterization of a TCP in terms of the operating discharge parameters such as pressure and power. One of the most important plasma diagnostic tools is the Langmuir probe. However, in a RF discharge, a Langmuir probe system to measure the electron energy distribution, density and temperature can be designed and utilized only if the magnitude of the plasma RF potential is known. Thus, the RF potential measurement is the first step in the use of a Langmuir probe measurement. Moreover, the design of a Langmuir probe requires a knowledge of the gas temperature, since it provides useful information about the materials that can be used in the measured range of temperature.

This report is divided in two parts. In the first part is described the plasma potential measurement, and the second part is focused on the temperature measurement.

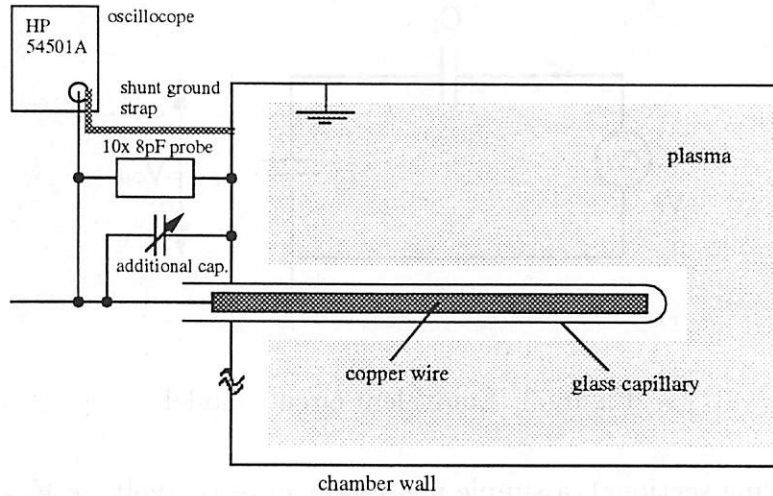


Figure 2: Experimental apparatus

## Part I: RF Plasma Potential Measurement

### 2 Experimental Apparatus

The instruments used to perform this measurement are quite simple. A glass capillary (12 in. long and 0.25 in. outside diameter) was introduced into the reactor chamber. Inside the glass, a copper wire of 0.137 in. in diameter and 9 in. in length was used as voltage detector, as shown in figure 2.

The plasma was powered at 13.56 MHz with a 1 kW Henry 1000D Radio Frequency Power Generator connected to an L-type capacitive matching network, as described by Gudmundsson and Lieberman [4].

The RF voltage between the copper wire and the ground was measured with an *HP 54501A* digitizing oscilloscope through a low capacitance passive probe (*HP 10430A*) of 8 pF input capacitance calibrated at 13.56 MHz. This voltage differs from the actual plasma voltage due to the capacitive coupling between the plasma and the wire (we refer to this coupling as the plasma capacitance,  $C_p$ ). As shown in figure 3, this coupling and the capacitance of the wire with respect to ground make the detecting system equivalent to a voltage divider. Since the exact value of  $C_p$  is not known (an approximate estimate of  $C_p$  is

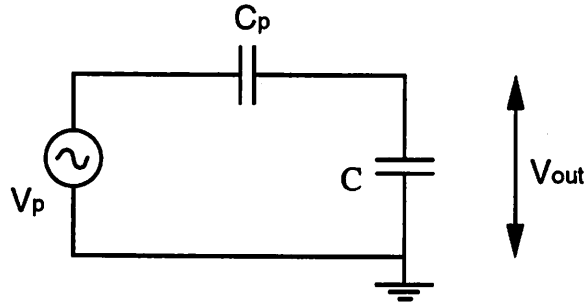


Figure 3: Equivalent circuit model

given in the following sections), a simple measurement of the voltage  $V_{out}$  is not sufficient to find the plasma potential.

From figure 3, applying the usual rule for a voltage divider, we get

$$V_{out} = \frac{C_p}{C_p + C} V_p$$

This equation makes clear why a low capacitance probe is used in the voltage measurement. It will be shown that the numerical value of  $C_p$  is around 50 pF. On the other hand,  $C$  is given by the sum of the stray capacitance of the copper wire to ground plus the input capacitance of the scope probe (8 pF), and a reasonable estimate of its value is above 30 pF. Therefore,

$$V_{out} \leq 0.6 V_p$$

Since the smaller is the value of the voltage  $V_{out}$  the more sensitive is the measurement to the noise, particular attention is used to reduce the value of  $C$ . Placing the oscilloscope input terminal as near as possible (approximately 8 in.) to the glass tube (thus shortening the cable length) was an additional procedure used to minimize the sensitivity of the measurement to 13.56 MHz noise pickup.

### 3 Voltage Calculation

From the circuit model of the measuring apparatus we see that the values of the plasma voltage  $V_p$  and the plasma capacitance  $C_p$  are unknown, and this makes it impossible to find  $V_p$  by merely measuring  $V_{out}$ . However,  $V_p$  can be calculated if the measurement is

performed for two different values of the capacitance  $C$ :  $C_1$  and  $C_2$ . (This can be done by adding a small capacitor connected from the copper wire to the ground, as shown in figure 2). We have then:

$$V_{out} = V_1 = \frac{C_p}{C_p + C_1} V_p$$

$$V_{out} = V_2 = \frac{C_p}{C_p + C_2} V_p$$

Therefore,

$$C_p (V_p - V_1) = C_1 V_1$$

$$C_p (V_p - V_2) = C_2 V_2$$

Dividing the left and right hand side of the preceeding equations, we get:

$$\frac{V_p - V_1}{V_p - V_2} = \frac{C_1 V_1}{C_2 V_2}$$

from which,

$$V_p = \frac{(C_1 - C_2) V_1 V_2}{C_1 V_1 - C_2 V_2}$$

## 4 Experimental Data

The voltage  $V_{out}$  was measured using different values for the capacitance  $C$ . The first measurement was done by simply connecting the copper wire to the low capacitance (8 pF) probe. Then, a small capacitance was added between the copper wire and the ground (thus increasing the value of  $C$ ). The following capacitors have been used: 10 pF, 22 pF, 49 pF. Hence, the experiment was performed with the following values for  $C$ :

8 pF	18 pF	30 pF	57 pF
------	-------	-------	-------

For each value of  $C$ , the peak-to-peak voltage  $V_{out}$  was measured versus pressure and absorbed power. The unprocessed raw data obtained are given in figure 4.

Berkeley, 4 Aug. 1995

MEASUREMENT #1  
data with a capacitance of 8 pF

Power (W)	Pressure (m Torr)		
	10	30	50
50	7.16	5.68	4.07
100	5.02	4.24	4.24
200	6.32	6.63	8.5
300	8.63	10.91	12.73
400	9.23	12.28	10.01
500	8.53	8.43	6.83

MEASUREMENT #2  
data with a capacitance of 18 pF

Power (W)	Pressure (m Torr)		
	10	30	50
50	5.61	4.58	3.38
100	4.07	3.53	3.57
200	5.13	5.46	7
300	7.13	8.39	10.52
400	7.62	10.17	8.4
500	7.08	7.07	5.83

MEASUREMENT #3  
data with a capacitance of 30 pF

Power (W)	Pressure (m Torr)		
	10	30	50
50	4.54	3.71	2.73
100	3.46	2.92	2.97
200	4.32	4.52	5.83
300	5.98	7.09	8.86
400	6.47	8.55	7.08
500	5.97	5.94	4.9

MEASUREMENT #4  
data with a capacitance of 57 pF

Power (W)	Pressure (m Torr)		
	10	30	50
50	3.25	2.69	1.91
100	2.46	2.09	2.11
200	3.2	3.39	4.18
300	4.37	5.3	6.37
400	4.79	6.22	5.17
500	4.46	4.39	3.65

the voltage is given in volts (p-p)

Figure 4: Raw data

		pressure (mTorr)		
		10	30	50
power (W)	50	8.7	6.9	5.1
	100	6.0	5.1	5.1
	200	7.4	7.8	10.2
	300	10.2	12.6	15.2
	400	10.7	14.5	11.8
	500	9.9	9.9	8.0

Table 1: Plasma potential

The waveform read at the oscilloscope was not a simple sinusoid at 13.56 MHz, but higher harmonics were observed. Nevertheless, the component at 13.56 MHz was always highly dominant.  $V_p$  was found by substituting for  $V_1$  and  $V_2$  the value of  $V_{out}$  obtained using two different values of  $C$ .  $V_p$  was calculated using for  $C_1$  and  $C_2$  each possible combination of the values of  $C$  given in the preceding table, then the results obtained for  $V_p$  were averaged.

In the table 1 the averaged values of  $V_p$  are given (in volts, peak-to-peak) versus pressure and transmitted power. The transmitted power is the power that enters the matching network and it is given as the difference between the incident and the reflected power as read with a wattmeter connected between the power supply and the matching network.

The sources of errors in the voltage reading are several. In this experiment we found two main sources of errors: the first one is probably due to the heating of the chamber that leads to a sort of hysteresis in the reading of the voltages  $V_1$  and  $V_2$ ; the second one is due to the imprecision of the reading of the exact transmitted power (we used a *Bird Wattmeter 4522*), and especially at low power, differences of the order of 5-10 watts may cause a significant error in the measurement. The probable error can be estimated as in Beckwith *et al.* [5]:

$$\Delta V_p = 0.67 \sigma \approx 0.2 \text{ V}$$

where  $\sigma \sim 0.27$  V is the average standard deviation shown by  $V_p$ . Similarly, the maximum error <sup>1</sup> is given by

$$\Delta V_p^{max} = 3.29 \sigma \approx 0.9 \text{ V}$$

This is the order of magnitude of the error in the plasma voltage calculation.

It is possible to represent the experimental results for the plasma voltage versus input power and pressure in a contour plot, as shown in figure 5, and in a surface plot, as shown in figure 6. In these plots the experimental data have been smoothed with a numerical interpolation of order 2, done with *Mathematica*. From the contour plot and the surface plot of the plasma voltage it is evident that there exists two different operating regimes of the reactor, and the separation point is seen around 200-300 watts. This agrees with the theory of inductive discharges for which inductive source operation is possible only if the absorbed power <sup>2</sup> is above a certain minimum value. If this is not the case, then the discharge is predominantly capacitively driven. As we can see, this threshold value is found to be at a transmitted power of 200-300 watts.

## 5 Plasma Capacitance

The results obtained for the plasma potential make it possible to calculate the plasma capacitance  $C_p$ . It is easy to see that  $C_p$  is given by:

$$C_p = \frac{C_1 V_1}{V_p - V_1} = \frac{C_2 V_2}{V_p - V_2}$$

where  $C_1$  and  $C_2$  can be any of the values given in the previous section,  $V_1$  and  $V_2$  are the voltages  $V_{out}$  read at the oscilloscope for the respective capacitance, and  $V_p$  is the plasma potential that corresponds to that choice of  $C_1$  and  $C_2$ . As for  $V_p$ , the values obtained for  $C_p$  were averaged over all possible choices of  $C_1$  and  $C_2$ , and the result is given in the table 2 (the capacitance is given in pF):

As for the voltage calculation, the error in the calculation of the plasma capacitance can be estimated. Since the average standard deviation is  $\sigma \sim 3.2$  pF, the probable error

---

<sup>1</sup>The probability that the deviation of the plasma voltage from its mean value is within the maximum error is 99.9%

<sup>2</sup>The absorbed power is the power that actually goes into the plasma. This differs from the transmitted power since the losses in the matching network and in the coil are not taken into account.

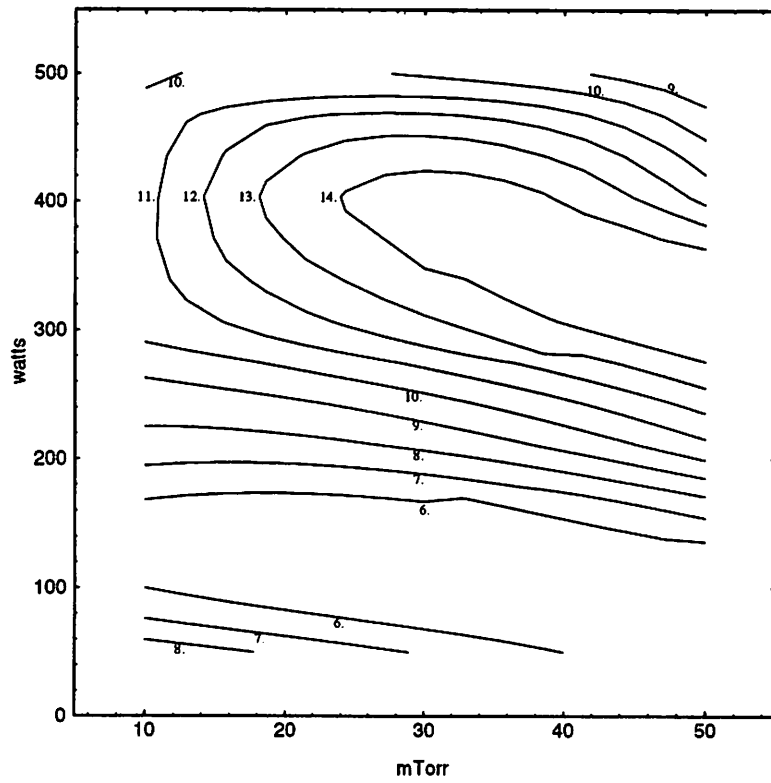


Figure 5: Plasma potential (p-p), experimental (with smoothing)

		pressure (mTorr)		
		10	30	50
power (W)	50	32.9	35.8	35.1
	100	40.5	39.7	40.9
	200	42.8	42.9	39.7
	300	42.5	40.4	41.7
	400	45.4	42.6	44.6
	500	45.7	45.2	48.0

Table 2: Plasma capacitance

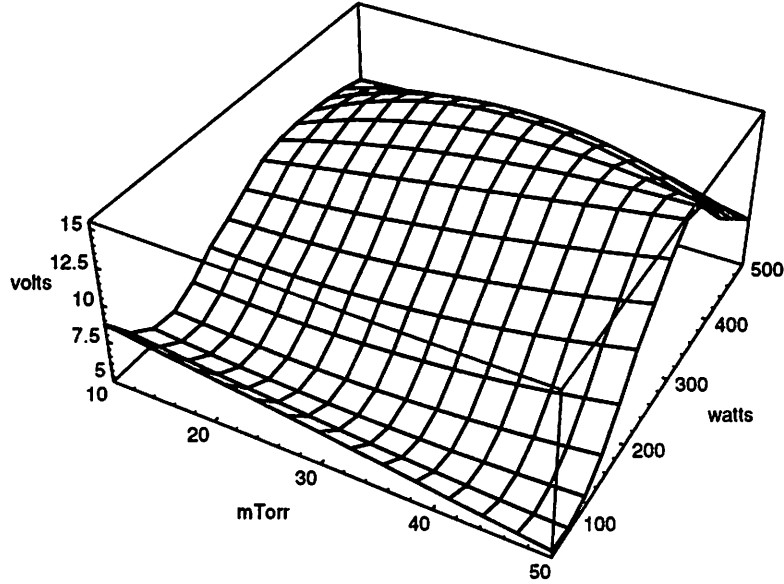


Figure 6: Plasma potential (p-p), experimental (with smoothing)

is obtained

$$\Delta C_p = 0.67 \sigma \approx 2.1 \text{ pF}$$

and the maximum error is given by

$$\Delta C_p^{max} = 3.29 \sigma \approx 10.5 \text{ pF}$$

What we call the plasma capacitance  $C_p$  is actually the series connection of three distinct terms: the sheath capacitance ( $C_{sh}$ ), the glass capacitance ( $C_g$ ) and the capacitance of the air gap between the copper tube and the glass ( $C_a$ ). Therefore,  $C_p$  is given by

$$C_p = \left( \frac{1}{C_{sh}} + \frac{1}{C_g} + \frac{1}{C_a} \right)^{-1}$$

Hence, the calculation of the plasma capacitance requires a knowledge of the sheath thickness which depends on the electron temperature and electron density inside the chamber. If we assume that the sheath thickness is small enough, then the value of the sheath capacitance may be much higher than the glass capacitance and the air gap capacitance; therefore, the contribution of  $C_{sh}$  should be negligible. As we will see in the next section.

this approximation is not quite true, since, especially at low power and pressure, the contribution of the sheath capacitance is important. However, in our simplified calculation, the plasma capacitance is given by the series connection of the glass capacitance and the air gap capacitance:

$$C_{p0} = \frac{C_a C_g}{C_a + C_g}$$

The glass tube capacitance,  $C_g$ , can be estimated

$$C_g = \frac{2\pi\kappa\epsilon_0 l}{\ln(d_{OD}/d_{ID})} \approx 73.5 \text{ pF}$$

and the air gap capacitance is given by

$$C_a = \frac{2\pi\epsilon_0 l}{\ln(d_{ID}/d_c)} \approx 154.8 \text{ pF}$$

where

$$l = 15 \text{ cm (glass tube length inside the chamber)}$$

$$d_{OD} = 0.25 \text{ in} = 0.635 \text{ cm (glass tube OD)}$$

$$d_{ID} = 0.15 \text{ in} = 0.381 \text{ cm (glass tube ID)}$$

$$d_c = 0.142 \text{ in} = 0.361 \text{ cm (copper tube diameter)}$$

$$\kappa = 4.5 \text{ (for the glass)}$$

Substituting the appropriate numerical values, the plasma capacitance is

$$C_{p0} \approx 49.8 \text{ pF}$$

This value is larger than the obtained experimental values, and this suggests that the contribution due to the sheath capacitance is not negligible. However, at high power and pressure, the approximation is closer to the experimental data, confirming that the sheath thickness, in this regime, should be much less than at low power and pressure.

A different estimate of  $C_{p0}$  can be obtained by extrapolation, in the following way. The sheath capacitance high power limit is given by

$$\lim_{P_{tr} \rightarrow \infty} C_{sh} = \infty$$

where  $P_{tr}$  is the transmitted power. Therefore, since

$$\frac{1}{C_p} = \frac{1}{C_{sh}} + \frac{1}{C_{p0}}$$

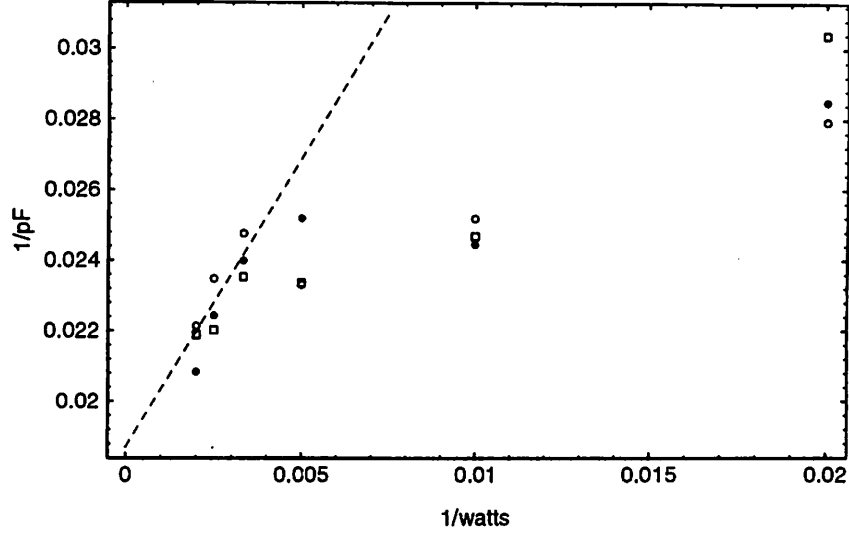


Figure 7: Inverse of plasma capacitance versus inverse of the power at 10 mTorr (boxes), 30 mTorr (circles), 50 mTorr (dots)

then, at high power,  $C_{p0}$  should be equal to  $C_p$ . In figure 7 the inverse of the plasma capacitance is plotted versus the inverse of the transmitted power  $P_{tr}$ . The value of  $C_{p0}$  can be found by a linear extrapolation of these points until they intersect the vertical axis  $1/P_{tr} = 0$ . The value of  $C_{p0}$  obtained varies slightly with pressure:

$$C_{p0} = \begin{cases} 52.4 \text{ pF,} & \text{at 10 mTorr} \\ 54.3 \text{ pF,} & \text{at 30 mTorr} \\ 53.4 \text{ pF,} & \text{at 50 mTorr} \end{cases}$$

Averaging,

$$C_{p0} \approx 53.4 \text{ pF}$$

## 6 Sheath Capacitance and Sheath Thickness

In this section we give a simplified calculation of the sheath capacitance and the sheath thickness. The sheath capacitance,  $C_{sh}$ , is given by

$$C_{sh} = \frac{2 \pi \epsilon_0 l}{\ln((d_{OD} + 2 s_m)/d_{OD})}$$

where  $s_m$  is the sheath thickness around the glass tube. We expect that in an inductive discharge the sheath thickness should be few Debye lengths. According to Godyak and Sternberg [6], the sheath thickness in the collisionless regime is given by

$$s_m = \lambda_{Des} (\delta + 1.375 \rho^2 + 0.3398 \rho^3)$$

where  $\lambda_{Des}$  is the Debye length at the sheath edge and  $\delta$  is given by

$$\delta = \frac{1}{6} \left( 2(2\eta_w + 1)^{1/2} - 1 \right)^{3/2} + \frac{1}{2} \left( 2(2\eta_w - 1)^{1/2} - \frac{2}{3} \right)$$

with

$$\eta_w = \ln \left( \frac{M}{2\pi m} \right)^{1/2}$$

where  $M$  is the ion mass and  $m$  is the electron mass. For argon  $\delta \approx 2.612$ . The parameter  $\rho$  that appears in the equation for the sheath thickness is a function of the fundamental RF voltage across the sheath  $V_{sh}$ . In particular,  $\rho$  is the positive root of the following equation [6]:

$$0.3398 \rho^4 + 1.375 \rho^3 + \delta \rho - \frac{V_{sh}}{T_e} = 0$$

The voltage  $V_{sh}$  is not known. However, since the sheath capacitance is considerably larger than the combined glass and air capacitance  $C_{p0}$  and the additional capacitance  $C$  (see figure 3), the voltage drop across  $C_{p0}$  and  $C$  is much larger than the one across  $C_{sh}$ . As first approximation we will assume  $V_{sh} \approx 0$ ; from which we get  $\rho \approx 0$  and

$$s_m \approx 2.612 \lambda_{Des}$$

with

$$\lambda_{Des} = 743 \sqrt{T_e/n_{es}}$$

( $T_e$  in V and  $n_{es}$  in  $\text{cm}^{-3}$ ). The density at the sheath edge  $n_{es}$  is related to the center density  $n_e$  by [7]

$$\frac{n_{es}}{n_e} = h_L = 0.86 \left( 3 + \frac{L}{2\lambda_i} \right)^{-1/2}$$

where  $L = 7$  cm is the chamber length and

$$\lambda_i \approx \frac{3.03}{p}$$

is the argon mean free path, with  $p$  (in mTorr) the gas pressure.

## 7 Global Model

Following Lieberman and Lichtenberg [7], it is possible to estimate the electron temperature  $T_e$  and the electron density  $n_e$  assuming a uniform density discharge model. In this model the electron temperature is found by particle balance, and  $T_e$  is given as solution of the equation

$$\frac{K_{iz}(T_e)}{u_B(T_e)} = \frac{1}{n_g d_{eff}}$$

where  $K_{iz}$  is the electron collision rate constant,  $u_B$  is the Bohm velocity,  $d_{eff}$  is an effective plasma size and  $n_g$  is the neutral gas density. We have [7]:

$$K_{iz} = K_{iz0} \exp\left(-\frac{\mathcal{E}_{iz}}{T_e}\right)$$

and

$$u_B = \left(\frac{e T_e}{M}\right)^{1/2}$$

where  $K_{iz0} \sim 10^{-7} \text{ cm}^3/\text{s}$ ,  $\mathcal{E}_{iz}$  is the ionization energy for argon ( $\sim 15.76 \text{ V}$ ),  $e$  is the electron charge and  $M$  is the argon mass. The gas density  $n_g$  is given as function of the background pressure  $p$ :

$$n_g = n^o \frac{p}{p^o}$$

where  $n^o$  is the Loschmidt's number and  $p^o$  is the standard pressure (760 Torr). For the particular chamber geometry (chamber radius of 15 cm and chamber length of 7 cm) and operating pressure regimes used in the experiment, the solution of the previous equation leads to the following result:

$$T_e = \begin{cases} 2.6 \text{ volts,} & \text{at } 10 \text{ mTorr} \\ 2.1 \text{ volts,} & \text{at } 30 \text{ mTorr} \\ 1.9 \text{ volts,} & \text{at } 50 \text{ mTorr} \end{cases}$$

Using the discharge power balance, the electron density  $n_e$  can be found:

$$n_e = \frac{P_{abs}}{e u_B A_{eff} \mathcal{E}_T}$$

where  $P_{abs}$  is the absorbed power,  $A_{eff}$  is a discharge effective area and

$$\mathcal{E}_T = 7.2 T_e + \mathcal{E}_c$$

is the total energy lost per ion lost from the system, where  $\mathcal{E}_c$  is the collisional energy loss per electron-ion pair created. The absorbed power  $P_{abs}$  is the power that is actually

absorbed by the plasma.  $P_{abs}$  is determined by measuring the transmitted power when there is plasma in the chamber and subtracting the transmitted power where there is no plasma, as pointed out by Gudmundsson and Lieberman [4]:

$$P_{abs} |_{I_{rf}} = P_{tr}^{plasma} |_{I_{rf}} - P_{tr}^{no\ plasma} |_{I_{rf}}$$

It is important to notice that these measurements must be done at the same applied current  $I_{rf}$  through the coil. For the chamber geometry and range of operating power and pressure used while running the experiment, we get

$$n_e \approx 2.70 \times 10^{10} - 4.47 \times 10^{11} \text{ cm}^{-3}$$

where the lower value was calculated with plasma at 10 mTorr and  $P_{tr} = 50$  W, and the higher one at 50 mTorr and  $P_{tr} = 500$  W. Furthermore, the density at the sheath edge is

$$n_{es} = h_L n_e = 6.21 \times 10^9 - 4.92 \times 10^{10} \text{ cm}^{-3}$$

At this point, an estimate of the Debye length at the sheath edge can be done:

$$\lambda_{Des} \approx 4.62 \times 10^{-3} - 1.52 \times 10^{-2} \text{ cm}$$

and also

$$s_m \approx 1.21 \times 10^{-2} - 3.97 \times 10^{-2} \text{ cm}$$

Similarly, the sheath capacitance can be calculated

$$C_{sh} \approx 71 - 223 \text{ pF}$$

Using the calculated value for  $C_{sh}$ , the plasma capacitance can be found. The result of this calculation is (using  $C_{p0} = 53.4$  pF)

$$C_p \approx 30 - 43 \text{ pF}$$

This range of values is in good agreement with the experimental values obtained for the plasma capacitance.

## 8 Electron Density

Since the values of the plasma capacitance are given by the experiment, we can use these values to find the sheath thickness and the electron density, thus reversing the analysis

		pressure (mTorr)		
		10	30	50
power (W)	50	0.0325	0.0254	0.0270
	100	0.0162	0.0176	0.0155
	200	0.0125	0.0124	0.0176
	300	0.0130	0.0164	0.0142
	400	0.0089	0.0128	0.0099
	500	0.0085	0.0091	0.0056

Table 3: Sheath thickness

done in the previous section. We have already seen that the plasma capacitance is given by

$$\frac{1}{C_p} = \frac{1}{C_{sh}} + \frac{1}{C_{p0}}$$

where

$$\frac{1}{C_{p0}} = \frac{1}{C_g} + \frac{1}{C_a}$$

Since  $C_{sh}$  is given as a function of the sheath thickness,  $s_m$ , we have

$$C_{sh} = \frac{2\pi\epsilon_0 l}{\ln((d_{OD} + 2s_m)/d_{OD})} = \frac{C_p C_{p0}}{C_{p0} - C_p}$$

Solving for  $s_m$ :

$$s_m = \frac{d_{OD}}{2} \left( \exp \left( \frac{2\pi\epsilon_0 l (C_{p0} - C_p)}{C_p C_{p0}} \right) - 1 \right)$$

Substituting the values for the numerical constants (using  $C_{p0} = 53.4$  pF), and neglecting higher order terms, the expression for the sheath thickness simplifies to

$$s_m \approx 0.318 \left( \exp \left( \frac{8.345}{C_p} - 0.156 \right) - 1 \right) \text{ cm } (C_p \text{ in pF})$$

The calculation of the sheath thickness is done and the results (in cm) versus transmitted power and pressure are given in table 3:

From table 3, we can see that the sheath thickness decreases with power and pressure. These results are consistent with the theoretical values of the sheath thickness estimated

		pressure (mTorr)		
		10	30	50
power (W)	50	$4.1 \times 10^{10}$	$8.7 \times 10^{10}$	$9.0 \times 10^{10}$
	100	$1.7 \times 10^{11}$	$1.8 \times 10^{11}$	$2.7 \times 10^{11}$
	200	$2.8 \times 10^{11}$	$3.7 \times 10^{11}$	$2.1 \times 10^{11}$
	300	$2.6 \times 10^{11}$	$2.1 \times 10^{11}$	$3.2 \times 10^{11}$
	400	$5.5 \times 10^{11}$	$3.4 \times 10^{11}$	$6.7 \times 10^{11}$
	500	$6.0 \times 10^{11}$	$6.8 \times 10^{11}$	$2.1 \times 10^{12}$

Table 4: Electron density

in the previous sections. The calculation of the error is carried out in the following way:

$$\Delta s_m = \sqrt{\left(\frac{\partial s_m}{\partial C_p}\right)^2 (\Delta C_p)^2 + \left(\frac{\partial s_m}{\partial C_{p0}}\right)^2 (\Delta C_{p0})^2}$$

thus,

$$(\Delta s_m)^2 \approx \left(\frac{0.0265 \exp(8.345/C_p - 8.345/C_{p0})}{C_p^2}\right)^2 (\Delta C_p)^2 + \left(\frac{0.0265 \exp(8.345/C_p - 8.345/C_{p0})}{C_{p0}^2}\right)^2 (\Delta C_{p0})^2$$

If we assume  $\Delta C_p \sim 2$  pF and similarly  $\Delta C_{p0} \sim 2$  pF<sup>3</sup>, then the average error on the sheath thickness calculation is of the order of 28%.

Since the sheath thickness is related to the Debye length, and the Debye length depends on the electron density, we can easily estimate the electron density, given the sheath thickness. Using for the sheath thickness the expression given in section 6 with no RF voltage across the sheath, we get

$$n_e = \frac{1}{h_L} T_e \left(\frac{1941}{s_m}\right)^2 \quad (s_m \text{ in cm})$$

The values obtained for the electron density (in cm<sup>-3</sup>) are given in table 4.

<sup>3</sup>Actually, there is no reason to believe that these errors should be the same. However, since these are similar quantities, assuming equal errors seems to be a good first approximation approach.

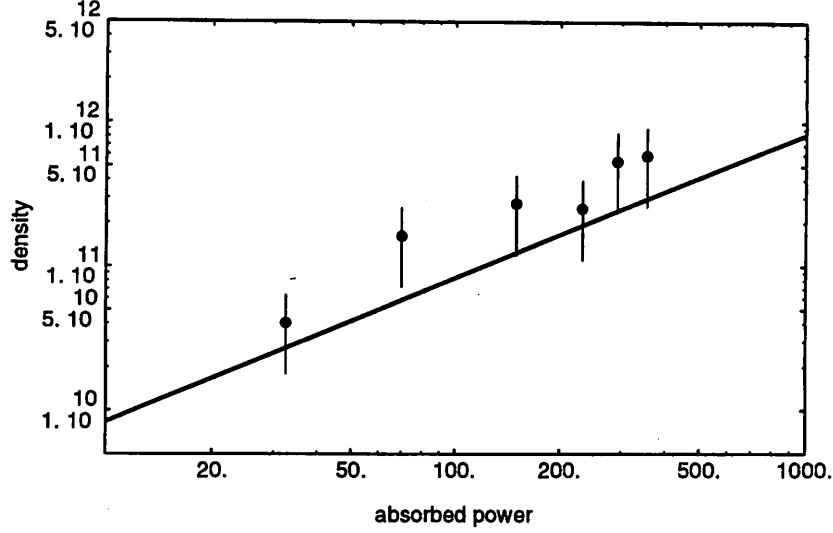


Figure 8: Electron density at 10 mTorr

These values for the electron density also agree with the theoretical estimate given by the global model. The error shown by the electron density is given by:

$$\Delta n_e = \left| \frac{\partial n_e}{\partial s_m} \right| \Delta s_m = \frac{T_e}{h_L} \frac{7.53 \times 10^6}{s_m^3} \Delta s_m$$

In figures 8, 9 and 10 the electron density (in cm<sup>-3</sup>) versus the absorbed power (in watts) is given, with the error on the electron density indicated. This error was calculated using  $\Delta s_m \sim 0.28 s_m$ ; hence,

$$\Delta n_e \approx \frac{T_e}{h_L} \frac{2.11 \times 10^6}{s_m^2}$$

As a comparison, the curve of the density obtained using the global model as described in the previous section is shown in these figures. We see that the electron density shows a clear dependence on power and pressure in agreement with the global model. In particular, the electron density increases almost linearly with absorbed power, in agreement with previous Langmuir probe measurements [3].

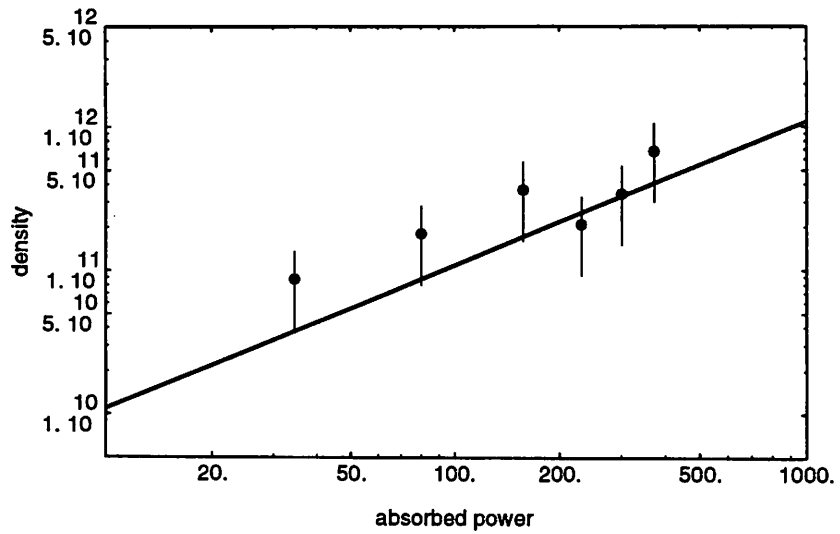


Figure 9: Electron density at 30 mTorr

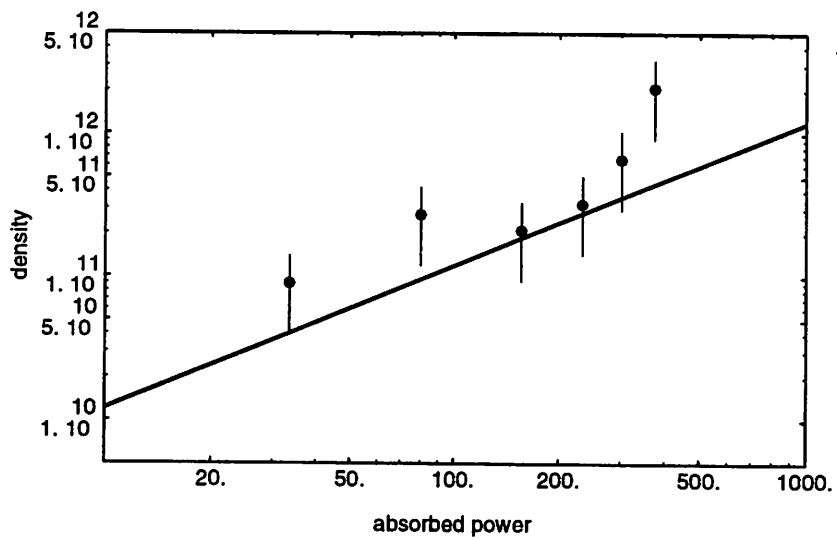


Figure 10: Electron density at 50 mTorr

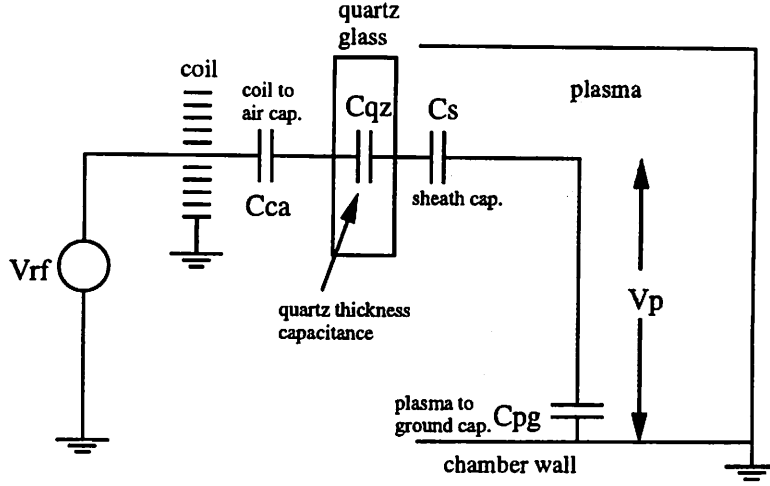


Figure 11: Plasma potential model

## 9 Approximate Modelling

It is interesting to look for an approximate expression for the plasma potential versus the gas pressure and the absorbed power.

In figure 11 is given a simple model that relates the driving RF voltage  $V_{rf}$  to the plasma potential  $V_p$ . The coil-to-air capacitance was measured experimentally to be

$$C_{ca} \approx 45.3 \text{ pF}$$

For the quartz glass capacitance we have:

$$C_{qz} = \frac{\kappa \epsilon_0 \mathcal{A}_w}{d_{qz}} \approx 55.89 \text{ pF}$$

where  $\kappa = 3.8$ , the thickness of the quartz plate is  $d_{qz} = 2.5 \text{ cm}$  and  $\mathcal{A}_w = 415.48 \text{ cm}^2$  is the surface area of the glass window. If we let  $C_0$  be the series connection of  $C_{ca}$  and  $C_{qz}$ , then we have  $C_0 \approx 25.02 \text{ pF}$ . The capacitance of the sheath in front of the glass window is

$$C_s = \frac{\epsilon_0 \mathcal{A}_w}{s_{m0}}$$

The sheath thickness  $s_{m0}$  depends upon the voltage drop  $V_s$  across the sheath. Letting  $V_0$  and  $V_s$  be the voltage drops across  $C_0$  and  $C_s$ , then

$$V_0 + V_s = V_{rf} - V_p$$

and also

$$C_0 V_0 = C_s V_s$$

from which we get

$$V_s = \frac{C_0 (V_{rf} - V_p)}{C_s + C_0}$$

The sheath thickness is then given as

$$s_{m0} = \lambda_{Des} \frac{V_{s1}}{T_e \rho(V_{s1})}$$

where  $V_{s1}$  is the fundamental amplitude of the voltage across  $C_s$  and  $\rho$  is a function of  $V_{s1}$  as given in section 6; therefore,

$$C_s = 4.95 \times 10^{-2} \frac{\rho(V_{s1})}{V_{s1}} (T_e h_L n_e)^{1/2} \text{ pF}$$

where  $n_e$  is given in  $\text{cm}^{-3}$ . The plasma-to-ground capacitance is given by

$$C_{pg} = \frac{\epsilon_0 \mathcal{A}_{ch}}{s_{m1}}$$

where  $\mathcal{A}_{ch} = 1582.6 \text{ cm}^2$  is the chamber wall surface area and  $s_{m1}$  can be written as

$$s_{m1} = \lambda_{Des} \frac{V_{p1}}{T_e \rho(V_{p1})}$$

where  $V_{p1}$  is the fundamental amplitude of the plasma voltage across the sheath. We have then,

$$C_{pg} \approx 0.19 \frac{\rho(V_{p1})}{V_{p1}} (T_e h_L n_e)^{1/2} \text{ pF}$$

Applying the usual rule of the voltage divider, we get

$$V_p = \frac{1}{1 + C_{pg} \frac{C_0 + C_s}{C_0 C_s}} V_{rf}$$

where  $V_p$  is the rms plasma voltage and  $V_{rf}$  is the rms driving voltage. The absorbed power  $P_{abs}$  scales with the rms driving current  $I_{rf}$  in the following way [4]:

$$P_{abs} = \rho_R I_{rf}^2$$

where  $\rho_R$  is the change of the coil resistance due to the plasma loading;  $\rho_R$  depends on the pressure and the input power. Similarly, since the coil is mostly inductive, the rms driving voltage is given by

$$V_{rf} = \omega L_s I_{rf}$$

where  $L_s$  is the coil inductance and  $\omega = 8.52 \times 10^7 \text{ s}^{-1}$  (13.56 MHz). Roughly, we can use the measured value  $L_s \sim 467 \text{ nH}$  [8]. Therefore, a relation between  $V_{rf}$  and  $P_{abs}$  is found

$$V_{rf} = \omega L_s \frac{P_{abs}^{1/2}}{\rho_R^{1/2}} \approx 39.8 \frac{P_{abs}^{1/2}}{\rho_R^{1/2}} \text{ V}$$

with  $P_{abs}$  given in watts and  $\rho_R$  in ohms. Gudmundsson and Lieberman [4] have determined an expression for  $\rho_R$  valid for argon plasma in the range of 10 to 60 mTorr:

$$\rho_R \approx 1 - \exp\left(-\frac{P_{abs}}{75.9}\right)$$

with  $10 \text{ W} < P_{abs} < 500 \text{ W}$ ;  $\rho$  does not change appreciably in our range of pressures, hence, in our approximation, it is considered independent of pressure.

## 10 Numerical Analysis

In the previous section we have developed in a simplified model the equations that describe the plasma voltage. These equation are repeated here. The rms plasma voltage is given by

$$V_p = \frac{1}{1 + C_{pg} \frac{C_0 + C_s}{C_0 C_s}} V_{rf} \text{ V}$$

with  $C_0 = 25.02 \text{ pF}$ ,

$$C_s = 4.95 \times 10^{-2} \frac{\rho(V_{s1})}{V_{s1}} (T_e h_L n_e)^{1/2} \text{ pF}$$

and

$$C_{pg} = 0.19 \frac{\rho(V_{p1})}{V_{p1}} (T_e h_L n_e)^{1/2} \text{ pF}$$

with  $\rho$  the positive root of

$$0.3398 \rho^4 + 1.375 \rho^3 + \delta \rho - \frac{V_{sh}}{T_e} = 0$$

with  $V_{sh}$  equal to  $V_{s1}$  or  $V_{p1}$  depending on the case. The rms voltage across  $C_s$  is given by

$$V_s = \frac{C_0 (V_{rf} - V_p)}{C_s + C_0}$$

with the rms driving voltage given by

$$V_{rf} = 39.8 \frac{P_{abs}^{1/2}}{\rho_R^{1/2}} \text{ V}$$

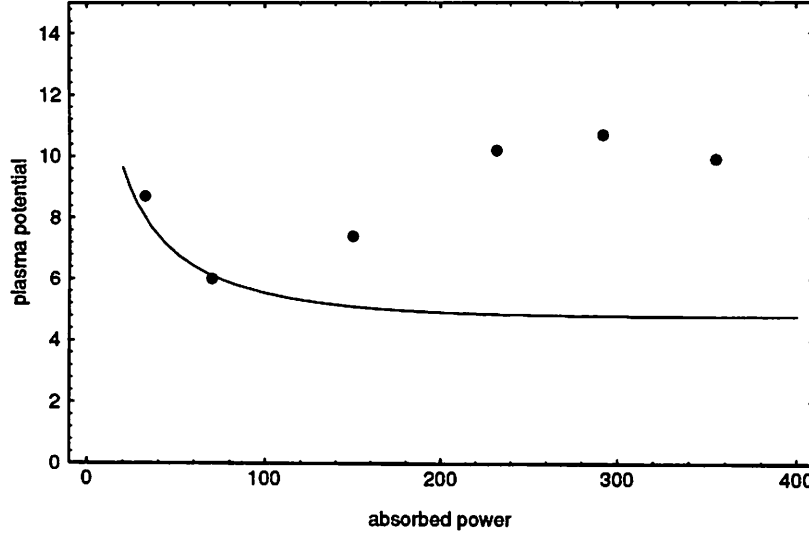


Figure 12: Plasma Potential vs Absorbed Power at 10 mTorr (dots are experimental values)

with

$$\rho_R \approx 1 - \exp\left(-\frac{P_{abs}}{75.9}\right)$$

We are interested in the plasma voltage  $V_p$  as a function of the pressure and the absorbed power. If  $p$  and  $P_{abs}$  are given, then, from the global model,  $h_L$ ,  $T_e$  and  $n_e$  can be found. However, this system of equations has to be solved iteratively. First a trial value for  $V_p$  and  $V_s$  is assigned. This allows us to find  $V_{p1}$  and  $V_{s1}$  as

$$V_{p1} = \sqrt{2} V_p$$

$$V_{s1} = \sqrt{2} V_s$$

( $V_{p1}$  and  $V_{s1}$  are amplitudes). Once we have them, given the pressure and the power, the equation for  $\rho$  can be solved and the values for  $C_{pg}$  and  $C_s$  are calculated. We are now able to find the new values for  $V_p$  and  $V_s$ . At this point the procedure is repeated until convergence is reached.

In figures 12, 13 and 14 the approximate result obtained for the plasma potential (in volts peak-to-peak) is plotted versus the absorbed power (in watts) for different values of the pressure. We can see that the theoretical model agrees with this experimental data at low absorbed power. In this regime the plasma is expected to be inductively coupled, but with a relatively high component of capacitive coupling also. At higher power, when

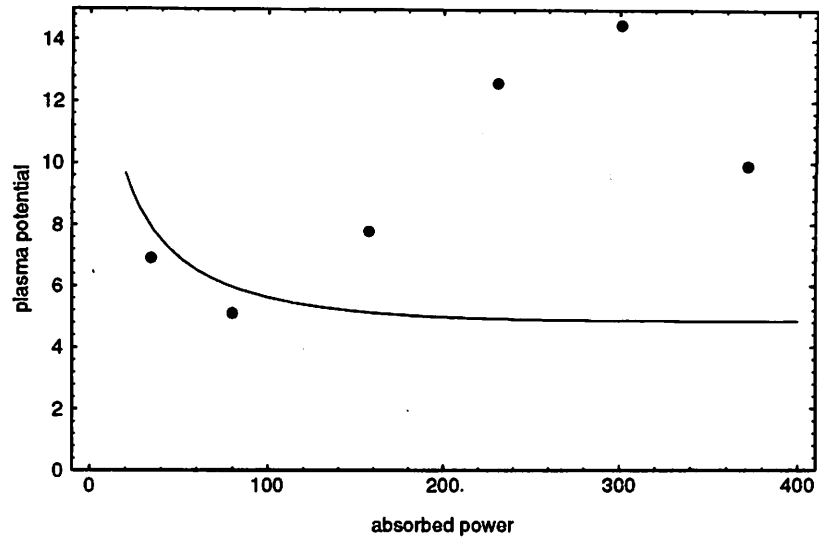


Figure 13: Plasma Potential vs Absorbed Power at 30 mTorr (dots are experimental values)

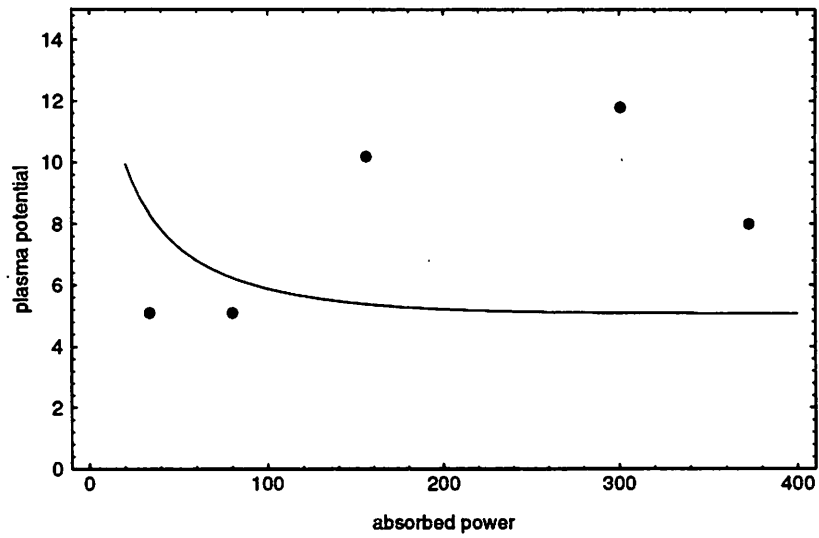


Figure 14: Plasma Potential vs Absorbed Power at 50 mTorr (dots are experimental values)

the plasma is inductively coupled and the capacitive coupling is weak, the experimental values diverge somewhat from the theoretical ones. The reasons for this divergence are not presently understood.

## Part II: Temperature Measurement

### 11 Experimental Apparatus

This measurement was performed by using a thermocouple introduced inside the same glass tube described in section 2. Thermocouples are based on the property that the electron density in metals depends on the temperature [9]. Therefore, a temperature difference across a pure metal wire will cause a net voltage between its edges. This voltage difference depends also on the material; hence, different metals will develop different voltages. As shown in figure 15,  $T_1$  is the temperature to be measured,  $T_2$  is a reference temperature, and  $V$  is the voltage difference that arises between the two junctions, since different metals are used. The choice of the two metals (or alloys) depends on temperature range of interest. Since we expect high temperature, a Chromel<sup>4</sup> – Alumel<sup>5</sup> thermocouple was chosen (this thermocouple is called *Type K*). In order to convert the thermocouple voltage to the temperature  $T_1$ , the temperature  $T_2$  must be known and constant. There are commercial devices that keep the reference junction at constant temperature and automatically convert the voltage  $V$  to the temperature  $T_1$  using appropriate calibration curves. In this experiment we used a *Fluke 51* to perform these operations. In addition, the thermocouple was tested at the freezing point and at the boiling point of the water, giving good readings.

Since the temperature is to be measured inside the reactor chamber, where the RF field can be very large, it was necessary to shield the thermocouple to avoid the RF pick-up that perturbs the temperature readings. The shielding apparatus is shown in figure 16.

---

<sup>4</sup>Chromel is an alloy of nickel with 10% chromium

<sup>5</sup>Alumel is an alloy of nickel with 2% aluminum, 2% manganese, and 1% silicon

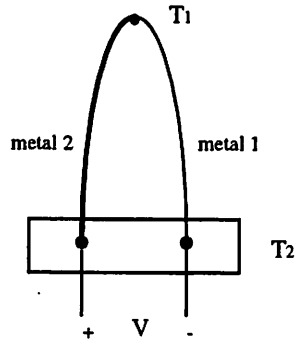


Figure 15: Thermocouple configuration (from [9])

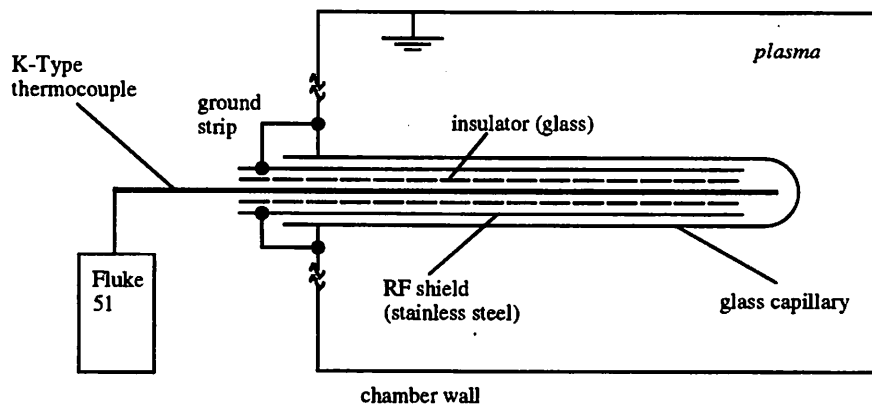


Figure 16: Experimental apparatus

		pressure (mTorr)		
		10	35	60
power (W)	50	83.9	102.7	111.2
	250	196.8	244.6	255.8
	500	287.4	336.5	355.5

Table 5: Surface temperature

## 12 Experimental Data and Analysis

The steady state surface temperature was measured at different transmitted powers and pressures, and the values obtained are given in table 5 (the temperature is given in degrees Celsius).

In figure 17 the temperature transient before it reaches the steady state is given for different operating conditions. It is clear that the steady state is reached approximately 30 minutes after the plasma is started.

As we can see from table 5, the steady state temperature increases with the transmitted power and pressure. Although these plasmas are characterized by a small ionization fraction ( $\sim 1\%$ ), it is believed [10] that ions and electrons bombarding the glass insulator contribute significantly to the measurement of the temperature. Hence we call this a *surface temperature* rather than a *gas temperature*. In the power and pressure range of interest, we can smooth the experimental data by a simple polynomial numerical fitting. We find:

$$T(p, P_{tr}) = T'_g(p, P_{tr}) = 21.8 + 1.99 p - 0.0205 p^2 + 0.797 P_{tr} + 0.00177 p P_{tr} - 0.000643 P_{tr}^2$$

where  $T = T'_g$  is the surface temperature measured, with  $P_{tr}$  given in watts,  $p$  given in mTorr and  $T$  in degrees Celsius. In figure 18 and 19 are given the surface and contour plot of  $T(p, P_{tr})$ . The relative error introduced by this numerical approximation is indeed very small, and it is possible to see that the average relative error is of the order of 2.1%.

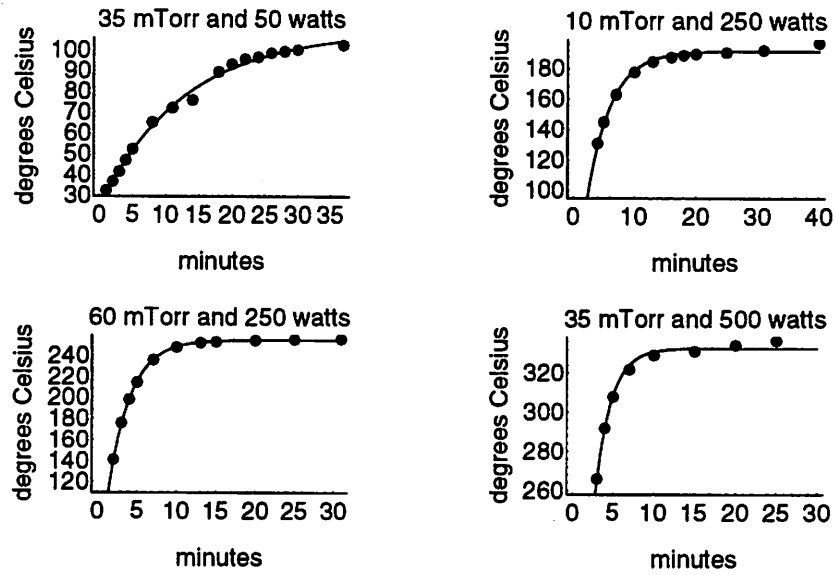


Figure 17: Temperature Transient

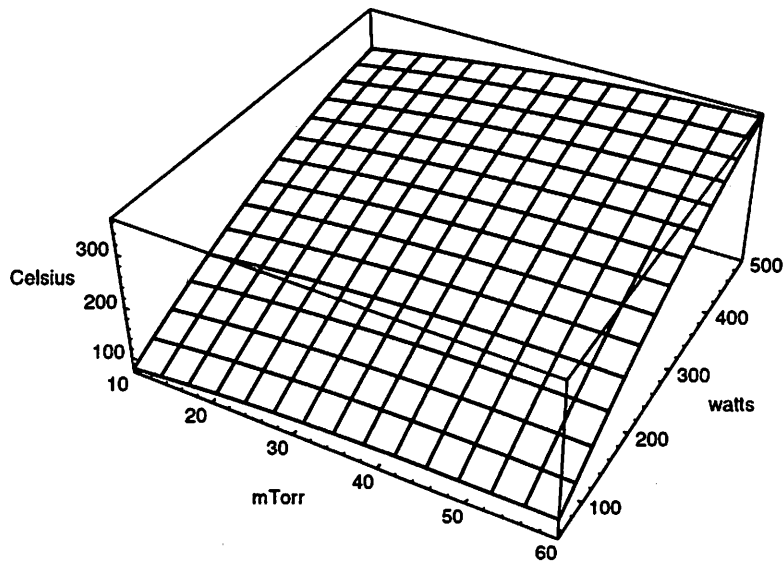


Figure 18: Surface temperature (C), surface plot

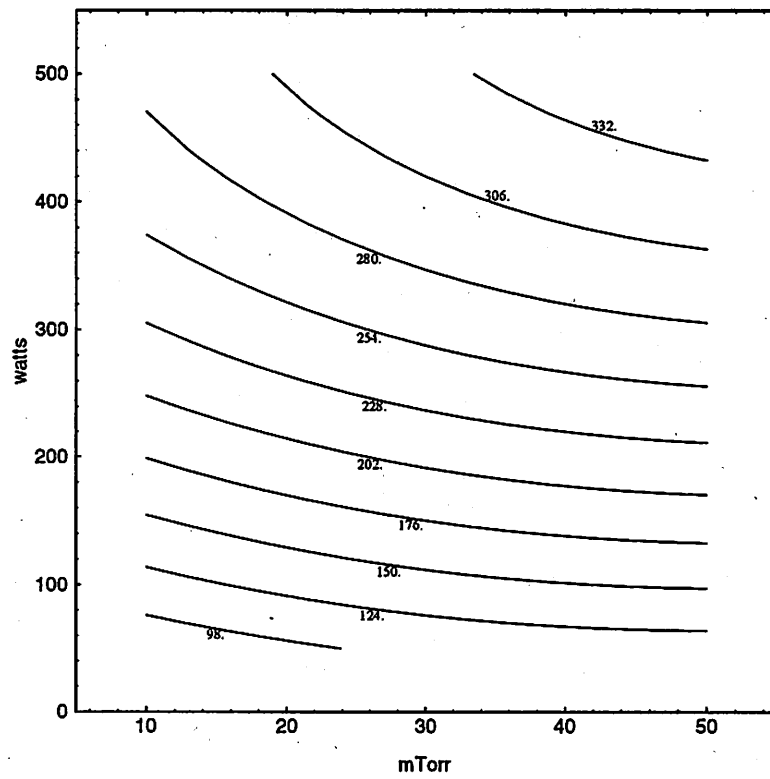


Figure 19: Surface temperature (C), contour plot

### 13 Heat Transfer Analysis

It is possible to give a simple thermodynamic model of the measuring apparatus, as shown in figure 20. In this model, we assume that the heat flux from the plasma to the glass capillary is predominantly along the radial direction. However, along the axis of the capillary, some heat is lost to the outside of the chamber through the glass tube, the stainless steel and the glass insulator, and  $T_{out}^{glass1}$ ,  $T_{out}^{ss}$  and  $T_{out}^{glass2}$  are their respective temperatures outside the reactor chamber. The contact resistance across the interface between the elements is also neglected. Following Lienhard [11], the radial thermal resistance is given by

$$R_{radial} = \frac{\ln(r_{OD}/r_{ID})}{2\pi k l}$$

where  $k$  is the thermal conductivity and  $l = 15$  cm is the tube length inside the plasma. Hence, from figure 21, the thermal resistance of the outside glass tube is

$$R_{radial}^{glass1} = \frac{\ln(r_4/r_3)}{2\pi k_{glass} l} \approx 0.42 \text{ K/W}$$

the stainless steel thermal resistance is given by

$$R_{radial}^{ss} = \frac{\ln(r_3/r_2)}{2\pi k_{ss} l} \approx 0.016 \text{ K/W}$$

and the glass insulator thermal resistance is

$$R_{radial}^{glass2} = \frac{\ln(r_2/r_1)}{2\pi k_{glass} l} \approx 0.49 \text{ K/W}$$

On the other hand, the axial thermal resistance is given by [11]:

$$R_{axial} = \frac{l}{\pi k (r_{OD}^2 - r_{ID}^2)}$$

Thus,

$$R_{axial}^{glass1} = \frac{l}{\pi k_{glass} (r_4^2 - r_3^2)} \approx 5650 \text{ K/W}$$

$$R_{axial}^{ss} = \frac{l}{\pi k_{ss} (r_3^2 - r_2^2)} \approx 2100 \text{ K/W}$$

$$R_{axial}^{glass2} = \frac{l}{\pi k_{glass} (r_2^2 - r_1^2)} \approx 23940 \text{ K/W}$$

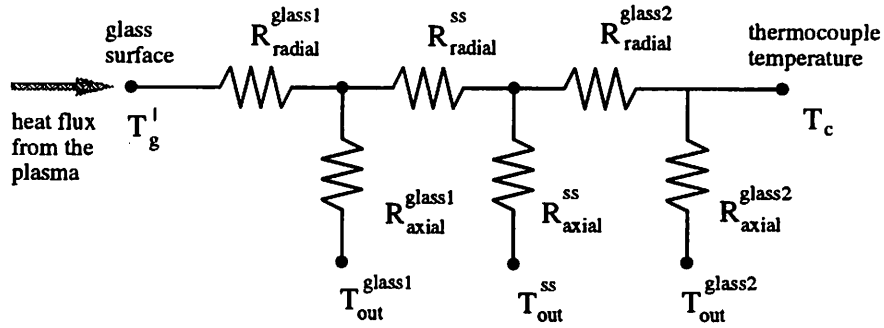


Figure 20: Thermodynamic model

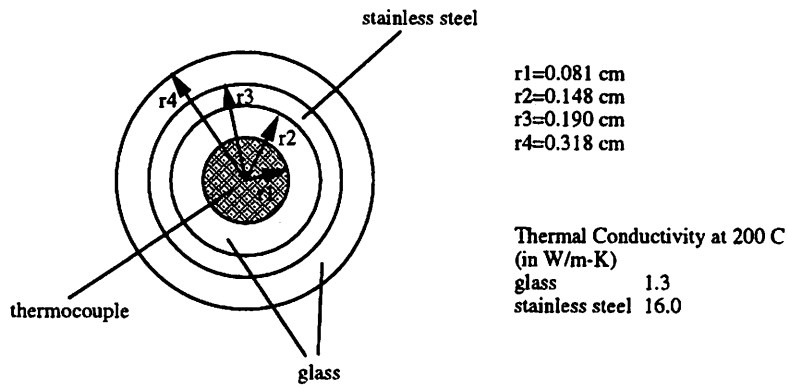


Figure 21: Radial section

As we can see, the axial resistances are much greater than the radial ones. Solving for the circuit given in figure 20, we get

$$T_c \approx 0.99 T'_g + 7.4 \times 10^{-5} T_{out}^{glass1} + 2.0 \times 10^{-4} T_{out}^{ss} + 1.7 \times 10^{-5} T_{out}^{glass2}$$

hence,

$$T_c \sim T'_g$$

where  $T'_g$  is the temperature on the glass surface inside the reactor chamber and  $T_c$  is the thermocouple temperature. This ensures that the introduction of the RF shield does not affect the temperature measurement.

## 14 Bulk Gas Temperature

The surface temperature  $T'_g$  is the temperature we measure with the thermocouple. However, this temperature is usually quite different from the bulk gas temperature. In a simple picture, we can assume that the power per unit volume delivered to the neutral argon atoms through collisions with electrons and ions is given by

$$P_{gas} = P_{el} + P_{ion}$$

with

$$P_{el} = \frac{2m}{M} K_{en} n_e n_g \frac{3}{2} e T_e$$

where  $2m/M$  is the average fraction of energy transferred in a collision between electron and neutral atoms and  $K_{en}$  ( $\sim 10^{-7}$  cm<sup>3</sup>/s, for argon) is the electron-neutral collision rate constant. The term due to ion-neutral collisions is given by

$$P_{ion} = \sigma_i \left( \frac{2e \mathcal{E}_{ic}}{M} \right)^{1/2} n_i n_g e \mathcal{E}_{ic}$$

where  $\sigma_i \sim 10^{-14}$  cm<sup>2</sup> is the ion-atom scattering cross section,  $\mathcal{E}_{ic}$  is the average ion energy in a collision with a neutral atom and  $n_i$  is the ion density (in a electropositive discharge  $n_i \sim n_e$ ). The average ion energy is found to be [7]

$$\mathcal{E}_{ic} \approx 0.62 \frac{1}{n_g \sigma_i} \frac{T_e}{z'}$$

where  $z'$  is a reduced wall separation (we will find  $z' = 6.59$  cm). For a simple estimate of  $P_{gas}$  we take  $T_e \sim 2.2$  V, thus

$$P_{gas} \approx 1.5 \times 10^{-30} n_e n_g + 3.3 \times 10^{-8} n_e n_g^{-1/2} \text{ W/cm}^3$$

where  $n_e$  and  $n_g$  are given in cm<sup>-3</sup>. Following Piejak *et al.* [10], the steady state gas temperature profile is determined by the solution of the heat transfer equation

$$\nabla^2 T_g + \frac{P_{gas}}{k} = 0$$

where  $T_g$  is the gas temperature and  $k$  is the thermal conductivity of the gas. The general solution of this equation is given by

$$T_g(\mathbf{r}_1) = \frac{1}{4\pi k} \int \frac{P_{gas}(\mathbf{r}_2)}{|\mathbf{r}_1 - \mathbf{r}_2|} d\tau_2$$

where the integral is taken over the volume of the discharge. We determine an approximate solution by neglecting the variation of  $n_g(\mathbf{r})$  with temperature in the power source term. It is possible to reduce this problem to one dimension by introducing a reduced wall separation  $z'$  [10] given by

$$\left(\frac{\pi}{z'}\right)^2 = \left(\frac{\pi}{z}\right)^2 + \left(\frac{2.405}{r}\right)^2$$

For  $z = 7$  cm (chamber length) and  $r = 15$  cm (chamber radius), we find a reduced wall separation  $z' = 6.59$  cm. The discharge geometry is then simplified as a one dimensional two plate discharge, with the plates located at  $\pm z'/2$ . Assuming the following spatial dependence of the power input into the discharge

$$P_{gas}(x) = P_{gas} \left(1 - \left(\frac{2x}{z'}\right)^2\right)$$

(with  $-z'/2 < x < z'/2$ ) we find [10]

$$T_{bulk} - T_w = \frac{5 P_{gas} z'^2}{48 k}$$

where  $T_{bulk}$  is the gas temperature at the center of the chamber and  $T_w$  is the chamber temperature on the inner wall. The gas atom mean free path is given by [12]

$$\lambda = \frac{7.3 T_{gas}}{10^{20} \pi r^2 p} \quad (\lambda \text{ in cm})$$

where  $r$  is the collision diameter for low energy collisions (for argon  $\pi r^2 \sim 3.67 \times 10^{-15}$  cm<sup>2</sup>) and  $p$  is the gas pressure (in Torr). Assuming  $T_{gas} = 295$  K (room temperature), we get

$$\lambda \approx \begin{cases} 0.59 \text{ cm,} & \text{at } 10 \text{ mTorr} \\ 0.10 \text{ cm,} & \text{at } 60 \text{ mTorr} \end{cases}$$

Therefore, in the pressure regime under which this experiment was run, the gas atom free path  $\lambda$  is much smaller than  $z'$ , and the thermal conductivity is a constant [13]. For argon

$$k = 1.9 \times 10^{-4} \frac{\text{W}}{\text{cm K}}$$

hence,

$$T_{bulk} - T_w \approx 3.5 \times 10^{-26} n_e n_g + 7.9 \times 10^{-4} n_e n_g^{-1/2}$$

In figure 22 ( $T_{bulk} - T_w$ ) is plotted versus the electron density for various gas pressures.

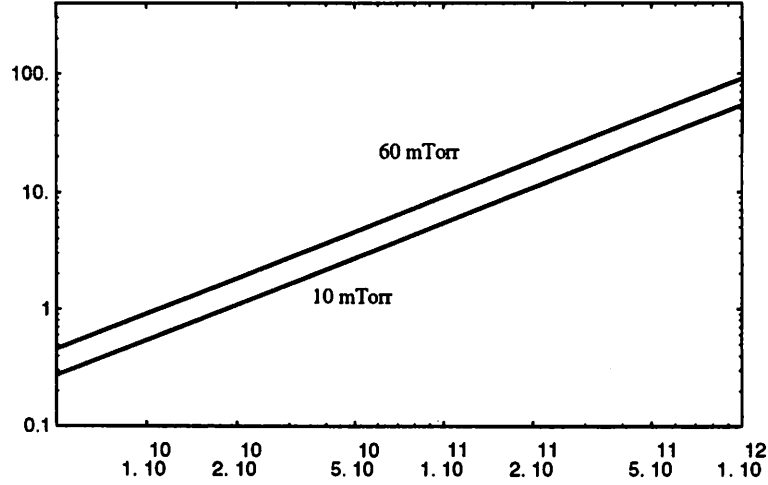


Figure 22:  $T_{bulk} - T_w$  (C) vs Electron Density ( $\text{cm}^{-3}$ )

## 15 Theoretical Model

We are interested in a model that relates the surface temperature with the discharge control parameters, pressure and power. In the steady state, the power flux into the thermocouple equals the power flux loss. Therefore, the energy balance equation is

$$S_{in} = S_{out}$$

where  $S_{in}$  is the power per unit area entering the thermocouple probe and  $S_{out}$  is the power flux loss.  $S_{in}$  is due to the charged (ions and electrons) and metastable atom particle flux on the glass surface of the probe<sup>6</sup>. Hence,

$$S_{in} = S_{charged} + S_{metastable}$$

with [7, 10]

$$S_{charged} \approx 0.61 e n_e u_B (2T_e + \mathcal{E}_i + \mathcal{E}_{iz})$$

$$S_{metastable} = \frac{1}{4} e n_m \gamma \left( \frac{8 k_B T_{bulk}}{\pi M} \right)^{1/2} \mathcal{E}_{ex}$$

<sup>6</sup>We will not consider the neutral particle flux as an energy flux into the thermocouple. However, since the bulk gas temperature is lower than the glass surface temperature, the neutral particles are heated up as they hit the glass surface. This is indeed an energy loss from the thermocouple.

where  $2T_e$  is the mean kinetic energy lost per electron lost (for Maxwellian electrons) and  $\mathcal{E}_i$  is the mean kinetic energy lost per ion lost,  $\mathcal{E}_{iz}$  is the ionization energy <sup>7</sup> (for argon  $\mathcal{E}_{iz} \sim 15.76$  V);  $n_m$  is the density of excited (metastable) neutral atoms,  $\gamma$  is the fraction of metastable atoms that de-excite and transfer their energy to the surface of the probe,  $k_B$  is the Boltzmann constant,  $\mathcal{E}_{ex}$  is the excitation energy ( $\sim 11.55$  V for argon) and  $M$  is the argon mass. A simple calculation (assuming  $T_e \sim 2.2$  V) yields

$$S_{charged} \approx 7.1 \times 10^{-13} n_e \text{ W/cm}^2$$

$$S_{metastable} \approx 1.1 \times 10^{-17} n_m \gamma T_{bulk}^{1/2} \text{ W/cm}^2$$

where  $T_{bulk}$  is given in kelvins. Ashida *et al.* [14] have calculated the metastable density of argon plasmas driven by time modulated power, and they found that the metastable density  $n_m$  has the same order of magnitude of the electron density  $n_e$ . Hence, we may assume  $S_{metastable} \ll S_{charged}$ .

The energy flux from the glass surface is mainly due to radiation and conduction through the stainless steel (at these low pressures, convection has no effects on heat transport) plus the thermal cooling due to the neutral particle flux.

$$S_{out} = S_{cond} + S_{rad} + S_{thermal}$$

Radiation heat flux is given by Stefan's Law:

$$S_{rad} = \epsilon_s \sigma (T_g'^4 - T_w^4)$$

( $T_g'$  and  $T_w$  in kelvins).  $T_g'$  is the gas surface temperature,  $\sigma$  is the Stefan-Boltzmann constant and  $\epsilon_s$  is the total emissivity of the probe surface ( $\epsilon_s \sim 0.85$  for the glass). However, the heat conduction through the stainless steel is negligible compared with the radiation heat loss. To see this, we note that

$$P_{cond} = \frac{T_g' - T_{out}^{ss}}{R_{axial}^{ss}}$$

Since  $R_{axial}^{ss} \approx 2100$  K/W and  $T_{out}^{ss}$  is not lower than the room temperature, then

$$P_{cond} \approx \begin{cases} 0.03 \text{ W,} & \text{at } T_g' = 83.9^\circ \text{ C} \\ 0.16 \text{ W,} & \text{at } T_g' = 355.5^\circ \text{ C} \end{cases}$$

---

<sup>7</sup>We assume that all the ions that hit the surface recombine with electrons.

On the other hand, the heat loss due to radiation can be evaluated as

$$P_{rad} = (2\pi r_4 l) S_{rad}$$

and assuming  $T_w \sim 50$  degrees Celsius, we get  $P_{rad} \approx 0.77$  W at low surface temperature and  $P_{rad} \approx 21.9$  W at high surface temperature. Therefore, the heat conduction term can be neglected and radiation seems to be the main heat loss process at low gas pressures [10, 15]. We have

$$S_{rad} \approx 4.8 \times 10^{-12} (T_g'^4 - T_w^4) \text{ W/cm}^2$$

The loss term due to the neutral particle flux can be found following Dushman. When the gas atoms hit the hot glass surface, energy is transferred from the surface to the atoms. Because we are in the regime where  $\lambda \approx r_4$ , the radius of the glass surface, we are in the transition between the low and high pressure thermal conduction regimes. As an estimate, we use the low pressure conduction theory. Hence [13]

$$S_{thermal} = \frac{1}{4} n_g \left( \frac{8 k_B T_{bulk}}{\pi M} \right)^{1/2} \alpha 2 k_B (T_g' - T_{bulk})$$

where  $\alpha$  is the accommodation coefficient, which takes into account the fact that for an atom usually several collisions with the glass surface are required for a complete energy transfer. For argon  $\alpha = 0.86$  [10], thus

$$S_{thermal} \approx 1.4 \times 10^{-22} n_g T_{bulk}^{1/2} (T_g' - T_{bulk}) \text{ W/cm}^2$$

At low power and low pressure we have  $n_e \sim 10^{10} \text{ cm}^{-3}$ ,  $n_g = 3.5 \times 10^{14} \text{ cm}^{-3}$ ,  $T_g' \approx 357$  K and  $T_{bulk} \approx 324$  K (assuming  $T_w = 50$  degrees Celsius); therefore

$$S_{rad} \approx 2.6 \times 10^{-2} \text{ W/cm}^2$$

$$S_{thermal} \approx 2.9 \times 10^{-5} \text{ W/cm}^2$$

Similarly, at high power and pressure,  $n_e \sim 10^{12} \text{ cm}^{-3}$ ,  $n_g = 2.1 \times 10^{15} \text{ cm}^{-3}$ ,  $T_g' \approx 630$  K and  $T_{bulk} \approx 404$  K (with  $T_w = 50$  degrees Celsius). Under these conditions

$$S_{rad} \approx 0.7 \text{ W/cm}^2$$

$$S_{thermal} \approx 1.3 \times 10^{-3} \text{ W/cm}^2$$

As we can see, in both cases  $S_{thermal}$  is much lower than  $S_{rad}$ . Therefore, it seems reasonable to neglect  $S_{thermal}$  in the energy balance equation.

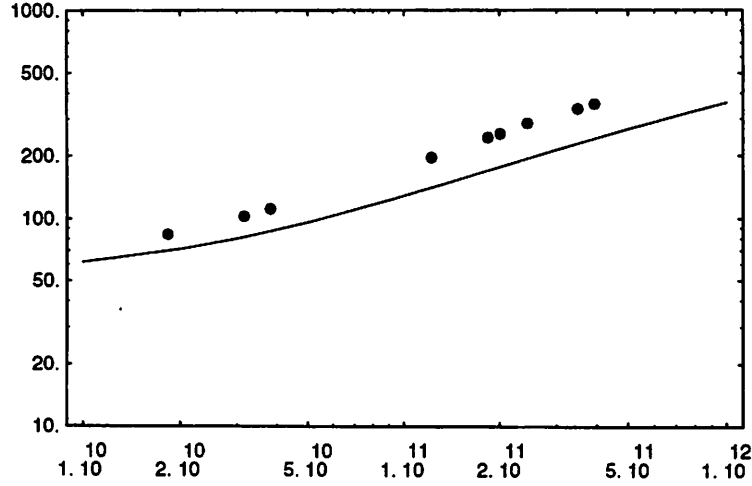


Figure 23: Surface Temperature (C) vs Electron Density (cm<sup>-3</sup>). The dots are experimental values.

The simplified energy equation which balance  $S_{charged}$  against  $S_{rad}$  becomes

$$7.1 \times 10^{-13} n_e \approx 4.8 \times 10^{-12} (T_g'^4 - T_w^4)$$

Rearranging, we get

$$T_g' \approx (T_w^4 + 0.15 n_e)^{1/4}$$

In figure 23  $T_g'$  is given versus the electron density (we have used  $T_w = 324$  K). In this plot we assumed that the plasma density at a certain power and pressure is the one given by the global model, as described in section 7. As we can see, the theoretical model we have developed gives in general slightly lower values for the glass surface temperature than the experimental measurements.

## 16 Conclusions

This experiment shows that a very simple (and inexpensive) probe can be used to measure the RF plasma potential. The results obtained seem to be fairly accurate, and able to reproduce some of the characteristics of an inductive plasma, such as a threshold power for inductive operation. Qualitative results for the plasma density were obtained, and the electron density roughly agrees with the analytical discharge model. It is also interesting

to see that the plasma potential appears to be fairly independent of the pressure, while showing variations with the input power. Similarly, the temperature measurement shows that the surface temperature is determined by balancing the charged particle energy flux against the radiation loss, such that the temperature increases with power and pressure.

The authors would like to thank D. Baca for experimental assistance.

## References

- [1] D.K. Coultas and J.H. Keller, European Patent, Publication No. 0 379 828 A2 (8 January 1990)
- [2] J.S. Ogle, U.S. Patent No. 4,948,458 (14 August 1990)
- [3] P.N. Wainman, M.A. Lieberman, A.J. Lichtenberg, R.A. Stewart and C. Lee (1995) *J. Vac. Sci. Technol.* **A13**, 2464
- [4] J.T. Gudmundsson and M.A. Lieberman (1996) *A Simple Transformer Model Applied to a Planar Inductive Plasma Discharge*, Memorandum No. UCB/ERL M96/3. University of California, Berkeley
- [5] T.G. Beckwith, R.D. Marangoni and J.H. Lienhard V (1993) *Mechanical Measurements*, Addison-Wesley, Reading (MA), *fifth edition*
- [6] V.A. Godyak and N. Sternberg (1990) *Phys. Rev. A.* **42**, 2299
- [7] M.A. Lieberman and A.J. Lichtenberg (1994) *Principles of Plasma Discharges for Materials Processing*, John Wiley and Sons, New York
- [8] D. Whiteson (1995) *An RF Voltage Divider for an Inductively Powered Plasma Source*, Memorandum No. UCB/ERL M95/61, University of California, Berkeley
- [9] J.H. Moore, C.C. Davis, and M.A. Coplan (1989) *Building Scientific Apparatus, Guide to Design and Construction*, Addison-Wesley, Reading (MA), *second edition*
- [10] R. Piejak, V. Godyak and B. Alexandrovich (1995) *Surface Temperature Measurements in Inductive Discharges in Xenon and Argon*, Osram Sylvania Inc., Beverly, MA. (Preprint)

- [11] J.H. Lienhard (1981) *A Heat Transfer Textbook*, Prentice-Hall, Englewood (NJ), *second edition*
- [12] P.A. Redhead, J.P. Hobson and E.V. Kornelsen (1968) *The Physical Basis of Ultrahigh Vacuum*, Chapman and Hall, London
- [13] S. Dushman (1949) *Scientific Foundations of Vacuum Techniques*, John Wiley and Sons, New York
- [14] S. Ashida, M.A. Lieberman and C. Lee (1995) *J. Vac. Sci. Technol.* **A13**, 2498
- [15] R.J. Visser (1989) *J. Vac. Sci. Technol.* **A7**, 189